ESCI upf.
School of International Studies

MEMÒRIA DEL TREBALL DE FI DE GRAU DEL GRAU DEL BDBI (ESCI-UPF)

Single-cell analysis of Plexiform Neurofibromas: Heterogeneity and tumor cell-of-origin

AUTOR/A: Pere Pericot Masdevall	NIA: 105514
GRAU: Bachelor's Degree in Bioinformatics	
CURS ACADÈMIC: 2021-2022	
DATA: 21/06/2022	
TUTOR/S: Bernat Gel Moreno / Eduard Serra Arenas	

ESCI upf. School of International Studies

Bachelor's Degree in Bioinformatics (UPF-UPC-UB-UAB)

Final Degree Project

Single-cell analysis of Plexiform Neurofibromas: Heterogeneity and tumor cell-of-origin

Pere Pericot Masdevall[1]

Scientific directors: Bernat Gel Moreno[1,2], Eduard Serra Arenas[1,3]

[1]Hereditary Cancer Group, Germans Trias i Pujol Research Institute (IGTP), Can Ruti Campus, Badalona, Spain

[2]Departament de Fonaments Clínics, Universitat de Barcelona (UB), Barcelona, Spain

[3]Centro de Investigación Biomédica en Red de Cáncer (CIBERONC), Madrid, Spain

Abstract

Neurofibromatosis type 1 (NF1) is a genetic disorder that, among other manifestations, predisposes affected persons to the development of tumors in the peripheral nervous system (PNS). These tumors arise due to the biallelic inactivation of the NF1 gene in a cell of the neural crest (NC) - Schwann cell (SC) lineage. One of these tumors are plexiform neurofibromas (pNFs), which are large benign tumors of the PNS that grow along large nerves and can compress vital structures. pNFs can transform towards an aggressive soft-tissue sarcoma, named malignant peripheral nerve sheath tumor (MPNST). The precise identity of the cell-of-origin of these tumors is still unknown, as well as which are the mechanisms that lie behind the process of malignization of pNFs towards MPNSTs. With new emerging genomic and bioinformatics technologies, such as single-cell genomics and epigenomics, many different possibilities to interrogate these tumors arise. However, we are still missing a profound dissection of this kind of data. The aim of this study is to perform an in-depth single-cell analysis of the transcriptional and genome accessibility profiles of pNFs, allowing for a better understanding of the underlying biological structure of these tumors. The results presented identified the expected cellular components with the expected proportions according to previous histological data. Interestingly, we found a significant degree of heterogeneity within cellular components. Together with other factors, heterogeneity within the SC component was partially explained by the presence of cells at diverse stages of differentiation within the NC-SC axis. Additionally, the study of the chromatin accessibility profiles of these cells has revealed that NC-SC differentiation not only implies transcriptional changes, but also epigenetic changes, which appear to be decoupled from one another. The analysis of single-cell tumor genomics and epigenomics provides further insights into tumor biology and may help us better understand their origin and malignization process.

Supplementary information: Supplementary material is available through the following link: https://drive.google.com/file/d/1Eft3aJylr9z80t6noVW8fppDS3FMjPHT/view?usp=sharing

1.- Introduction

Neurofibromatosis type 1 (NF1) is a tumor predisposition genetic disease that affects approximately 1 in 3,500 individuals worldwide, and is caused by the presence of a mutated copy of the NF1 tumor suppressor gene (Riccardi, 1992). Patients with NF1 show major clinical manifestations which involve the nervous system, the skin, and the skeletal system, implicating cells derived from the neural crest (NC). Although there exists a great variability in the different manifestations of the disease, the formation of tumors in the peripheral nervous system (PNS) is one of its most characteristic traits (Ferner, 2007). The NF1 gene encodes for a protein named neurofibromin, which is a RAS GTPase-activating protein that catalyzes the inactivation of RAS. Therefore, loss of NF1 results in activation of RAS and its downstream signaling pathways, which are key drivers of cancer, such as the MAPK/ERK kinase cascade.

Neurofibromin has also been found to be a regulator of cAMP-dependent pathways (Ratner & Miller, 2015).

There exist diverse NF1-related tumors that develop in the PNS, which are a major source of clinical complications for patients with the disease, all of which show biallelic inactivation of the NF1 gene (Brems et al., 2009). These tumors can be both benign or malignant, and include cutaneous neurofibromas (cNFs), plexiform neurofibromas (pNFs), atypical neurofibromas (aNFs), and malignant peripheral nerve sheath tumors (MPNSTs) (Serra et al., 2020).

More than 95% of patients with NF1 develop cNFs, which are benign tumors that originate in the PNS, forming discrete and well-circumscribed non-encapsulated nodules that never progress to malignancy (Ortonne et al., 2018). These neurofibromas arise due to the double inactivation of NF1 in Schwann cells (SCs). The interaction of these SCs with other *NF1(+/-)* cellular components facilitates the formation of the neurofibroma (Buchstaller et al., 2012; Serra, 2000). pNFs are also a common manifestation of the disease, observed as big neurofibromas that seem to arise during development. These benign tumors can potentially undergo malignant progression towards an MPNST (Ducatman et al., 1986). MPNSTs are soft tissue sarcomas that have a peripheral nerve sheath origin, and are aggressive tumors with high metastatic potential, which makes them key contributors to reduced life expectancy in patients with NF1 (Evans et al., 2011). The lifetime risk of developing an MPNST for an NF1 patient has been observed to be of about 10-15% (Uusitalo et al., 2016). The genomes of these tumors are typically hyperdiploid and highly rearranged, and complete resection by surgery is essential in current therapies to treat MPNSTs (Beert et al., 2011; Carli et al., 2005). In contrast with pNFs, which express markers from the Schwann cell lineage (such as SOX10, S100B, or CDH19), MPNSTs show a significant decrease in the expression of these genes (Miller et al., 2006), while showing an increase in the expression of mesenchymal markers (unpublished data). A very common path to malignancy in the progression from a pNF towards an MPNST is the generation of an atypical neurofibroma (aNF), described as distinct and slowly growing nodular lesions that exhibit histological features considered as pre-malignant, and hence being generally considered as precursor lesions of MPNSTs (Beert et al., 2011). In fact, it has been shown in the analysis of tissue samples capturing the pNF-MPNST progression that the same NF1 somatic mutation is shared between the MPNST and the pNF it arised from (Hirbe et al., 2015).

Plexiform neurofibromas (pNFs) are large and complex tumors that grow along large nerves and can compress vital structures. These tumors exhibit highest growth rates during early childhood (Dombi et al., 2007), and despite their non-metastatic and benign nature, they constitute a major source of substantial morbidity and account for an increased risk of mortality when symptomatic (Prada et al., 2012). pNFs can have a great impact on the quality of life of patients and, as mentioned previously, they may undergo malignant transformation towards an MPNST in some cases. The MEK inhibitor (MEKi) Selumetinib has been used in children with inoperable pNFs, reducing tumor volume by more than 20% in approximately 70% of the cases, lowering their pain and improving their overall quality of life (Dombi et al., 2016). This inhibitor has been approved by the FDA as the first ever treatment for NF1.

As reviewed in Mazuelas et al. (2020), pNFs are identified in around 50% of NF1 patients by using magnetic resonance imaging (MRI) (Mautner et al., 2008). Genetic analyses have pointed towards NF1 loss as the driver of plexiform neurofibroma tumorigenesis. Each pNF arises from an independent inactivation of this gene (Pemov et al., 2017). The cellular composition of these neurofibromas is the same as that of cNFs, although the identity of the cells that originate them and how they could impact

tumor development and composition could be different and is still a matter of discussion.

During embryo development, neural crest (NC) cells differentiate into Schwann cells (SCs) in a multi step differentiation process, which involves the generation of an intermediate population denominated as Schwann Cell Precursors (SCPs), which have the capacity to differentiate into immature SCs, which will then be able to form myelinating or non-myelinating mature Schwann cells (Mazuelas et al., 2022; Woodhoo & Sommer, 2008). There exists certain diversity within the different cellular types that compose a pNF, but such as with cNFs, *NF1*(-/-) Schwann cells and *NF1*(+/-) endoneurial fibroblasts are the main cell types, although perineurial cells, infiltrating immune cells, axons and others are also found within these tumors (Krone et al., 1983). To characterize the two main cellular components present in these tumors, there exist several known markers, including S100B, SOX10 and CDH19 for the Schwann cell (SC) lineage, with S100B known to be a marker for a more mature SC (Mazuelas et al., 2022), or PRRX1 and TWIST1 for a fibroblast component (Soldatov et al., 2019).

Different genetically modified mouse models (GEMMs) that develop pNFs have been generated, using the Cre-loxP system to ablate the NF1 gene in specific developmental cell stages of the NC-SC differentiation axis (Wu et al., 2008; Zheng et al., 2008; Zhu et al., 2002). These models, along with observing pNFs being formed after transplantation of NF1-deficient embryonic dorsal root ganglia / nerve root neurosphere cells to the sciatic nerve of nude mice points to Schwann Cell Precursors (SCPs) as the cells of origin for pNFs (Buchstaller et al., 2012; Chen et al., 2014). Moreover, a recent study has developed an *in vitro* 3D model for NF, based on the culture of iPSC-derived differentiating NF1*(-/-)* SCs along with primary NF1*(+/-)* pNF-derived fibroblasts, which can be engrafted in the sciatic nerve of nude mice and generate human NF-like tumors (Mazuelas et al., 2022).

2.- Objectives

This project will be developed under the hypothesis that the cell of origin of pNFs is not a mature SC but rather a less differentiated cell in the NC-SC axis such as a SCP or similar. On one hand, this could have implications regarding the cells constituting the whole SC component, potentially consisting of cells at different stages of maturation. On the other hand, this provides an opportunity to study the identity of these cells and assess whether this identity needs to change or not when progressing towards an MPNST.

This project aims to fulfill the following objectives:

1. To study and characterize the cellular diversity that exists within plexiform neurofibromas, as well as to determine the heterogeneity of Schwann cells that compose them.

2. To determine if there exist NF1(-/-) cells within pNFs with the potential to differentiate towards a mesenchymal phenotype, the existence of which would point towards them potentially being the cells originating MPNSTs.

3. To assess whether this same diversity is observed in iPSC-based *in vitro* 3D neurofibroma models or not.

3.- Methods

3.1 Patients and samples

Tumor samples were provided by diagnosed NF1 patients after giving written informed consent. They were obtained from three independent individuals after surgery of three plexiform neurofibromas (pNFs), labeled as: PNF19 (corresponding to a 45 year old female), PNF20 (corresponding to an 11 year old male), and PNF23 (corresponding to an 8 year old female). The pNF samples used in this project

were obtained by Mazuelas et al., 2022, and further details on the processing of the samples can be found there.

iPSC-based *in vitro* 3D neurofibroma models generated in the lab were processed following the same procedures as with the primary tumors, as described in Mazuelas et al., 2022. We analyzed 3 different models, all of them composed of 30% PNF-derived fibroblasts from the same patient, and 70% differentiating Schwann cells.

3.2 Single-cell data preparation and sequencing

Single cell RNA-seq data was obtained from the three pNF samples and the three different models as described in Mazuelas et al., 2022. Briefly, after dead cells were removed from the processed pNF samples, cells were resuspended in DMEM + 10% FBS (Gibco) + 1x GlutaMAX (Gibco), filtered with a 40µm filter and cell viability was calculated with the TC20™ Automated Cell Counter (Bio-Rad). Cells were run in the Chromium Single Cell Gene Expression (10X Genomics) in order to obtain the 3' transcriptome libraries to then be sequenced on an Illumina sequencer. This data was generated at the Centre Nacional d'Anàlisis Genòmics (CNAG), in Barcelona.

Independently, a combination of scRNAseq + scATACseq data only from the pNF samples described above was generated in the CNAG by using Chromium Single Cell Multiome ATAC + Gene Expression (10X Genomics), following vendor instructions.

3.3 Pre-processing and quality control

FASTQ files were processed with the CellRanger software (version 3.1.0) from 10X Genomics, by using the *count* pipeline with the pre-built human reference package (version 3.0.0). Downstream analysis was performed using R (version 4.1.1), Bioconductor (version 3.14) (Huber et al., 2015), and Seurat (Hao et al., 2021).

UMIs per gene per cell matrices were loaded into R by using DropletUtils (Griffiths et al., 2018). Standard quality control procedures and normalization were performed with scater (McCarthy et al., 2017), including the elimination of cells with low library sizes, low number of features, and high number of reads mapped to genes in the mitochondrial genome, as well as doublet detection and removal, which was done using scDblFinder (Germain et al., 2021). Also, batch correction was performed by applying mutual nearest neighbors (MNN) correction with the batchelor package (Haghverdi et al., 2018).

3.4 Single-cell RNA-seq analysis

For downstream analysis, we identified highly variable genes (HVGs) by selecting the top 20% most variable genes using scran (Lun et al., 2016). Subsequently, we performed dimensionality reduction by PCA and T-Distributed Stochastic Neighbor Embedding (TSNE), along with Uniform Manifold Approximation and Projection (UMAP), followed by a clustering based on a two-step procedure combining k-means and graph-based clustering using the infomap algorithm.

In order to assign cells to a predicted cell type, we performed cell type annotation using singleR (Aran et al., 2019) and the Human Primary Cell Atlas (Mabbott et al., 2013) as a reference. Additionally, to assess for significant differences in gene expression between different components of cells, differential expression (DE) analysis was performed with limma, using the *voom()* function (Ritchie et al., 2015), and gene-set enrichment analysis was done using ShinyGO (Ge et al., 2020). Plots for visualization of the analyses were generated using scater and ggplot2 (Wickham, 2016).

3.5 Signature scoring

Signature scoring was performed in order to assign scores to each cell based on their overall

expression of particular sets of genes that are characteristic of particular cell states using Seurat's *AddModuleScore()* function. These scores were then passed on to the original object and plotted using scater.

In order to assign cells to a particular cellular state, gene sets found to be upregulated in NC, Early SCs and Mature SCs (Mazuelas et al., 2022) were used to compute scores for each cell and gene set that were then normalized by L2-normalization. Each cell was assigned to the state with the highest normalized score if any of them was greater than 0.015.

3.6 RNA velocity

In order to perform RNA velocity analysis, we generated spliced and unspliced count matrices from the raw FASTQ files by using kallisto | bustools (Bray et al., 2016; Melsted et al., 2021). The data was loaded into the R environment using zellkonverter, and the analysis was performed with velociraptor, which performs the velocity calculations via the scVelo Python package (Bergen et al., 2019).

3.7 Single Cell Multiome ATAC + Gene Expression and analysis

To analyze the data generated from the 10X Genomics Multiome, FASTQ files were processed with the CellRanger ARC software (version 2.0.1) from 10X Genomics, by using the *count* and *aggr* pipelines with the pre-built human reference package (version 2.0.0).

Gene expression data was analyzed following the same procedures explained above. In the case of scATACseq data, standard quality control procedures were performed using Signac (Stuart et al., 2021), including nucleosome signal and TSS enrichment scoring, as well as checking for unusually low or high counts. Peak calling was performed using MACS2 (Zhang et al., 2008), and peak to gene links were predicted with Signac's *LinkPeaks()* function. Coverage plots to visualize the chromatin accessibility profiles of certain groups of cells were generated with the *CoverageBrowser()* function from Signac.

Code availability: All scripts used for the development of this project can be found at: https://github.com/pereperi/FDP

4.- Results and discussion

4.1 Quality control and sample cleaning

In order to begin with the treatment of the data from all pNF samples, consisting of 9092 (PNF19), 6155 (PNF20), and 5087 single cells (PNF23), standard quality control procedures and normalization were followed, which included the elimination of cells with low library sizes, low number of features, and high percentage of reads mapped to mitochondrial transcripts. However, other factors generating noise might appear during the processing of the samples, which is done separately, therefore giving place to a "batch effect", or to other cellular artifacts that may introduce false variation in the dataset such as cellular response to stress events which the cells can be subject to during the processing of the tumor samples.

After performing feature selection and dimensionality reduction, a strong batch effect was observed when plotting the cells in the reduced space by sample of origin. To deal with this, we applied mutual nearest neighbors (MNN) correction (Fig. 1A), which resulted in a more equally distributed visualization in which we could at first glance observe the presence of two main components of cells which expressed CDH19 on one hand and PRRX1 on the other (Fig. 1B), which are known to be markers for the Schwann cell lineage and for a mesenchymal phenotype, respectively.

Selecting only the component of cells expressing CDH19, we obtained a UMAP visualization which clearly separated the component in two, showing a cluster of cells that was predominantly composed of cells from one of the samples (PNF19) (Fig. 1C). After

performing a differential expression analysis between these two clusters, followed by an enrichment analysis using the resulting genes, we concluded that this separation could be caused by the presence of cells showing high levels of stress in the endoplasmic reticulum, which could also clearly be seen when plotting the scores of the GO:0034976 signature (Figs. 1C and S1).

We found that cells showing response to stress were present throughout the whole set of cells, and corresponded in the most part to those from PNF19 (Fig. 1D). In order to avoid confounding and future misleading results due to the variation this artifact might introduce, we eliminated cells showing response to stress in the endoplasmic reticulum from downstream analysis by getting rid of cells with a score >0.35 for the mentioned GO:0034976 signature (Fig. 1E).

The presence of a subpopulation of cells expressing both CDH19 and PRRX1 markers was of interest for us at first, regarding the possibility for them to potentially represent a less differentiated state capable of differentiating towards both identities. However, further diving revealed that this subpopulation had around 2X more reads on average than the rest of cells, so we applied procedures for doublet removal in order to deal with this artifact (Fig. S2).

The emphasis put on proper application of quality control was significant in order to remove undesired cellular artifacts and ensure the credibility of future results, since we noticed a lack for a proper standardized procedure in order to detect and eliminate the effect of stress or other artifacts that might appear during the processing of samples prior to being run in the Chromium. Moreover, the identification of this sample-specific cellular artifacts after batch correction gives strength to the fact that MNN correction does not assume the population composition is the same across samples and therefore does not "over-correct" the data, but instead still leaves the biological differences between samples at sight.

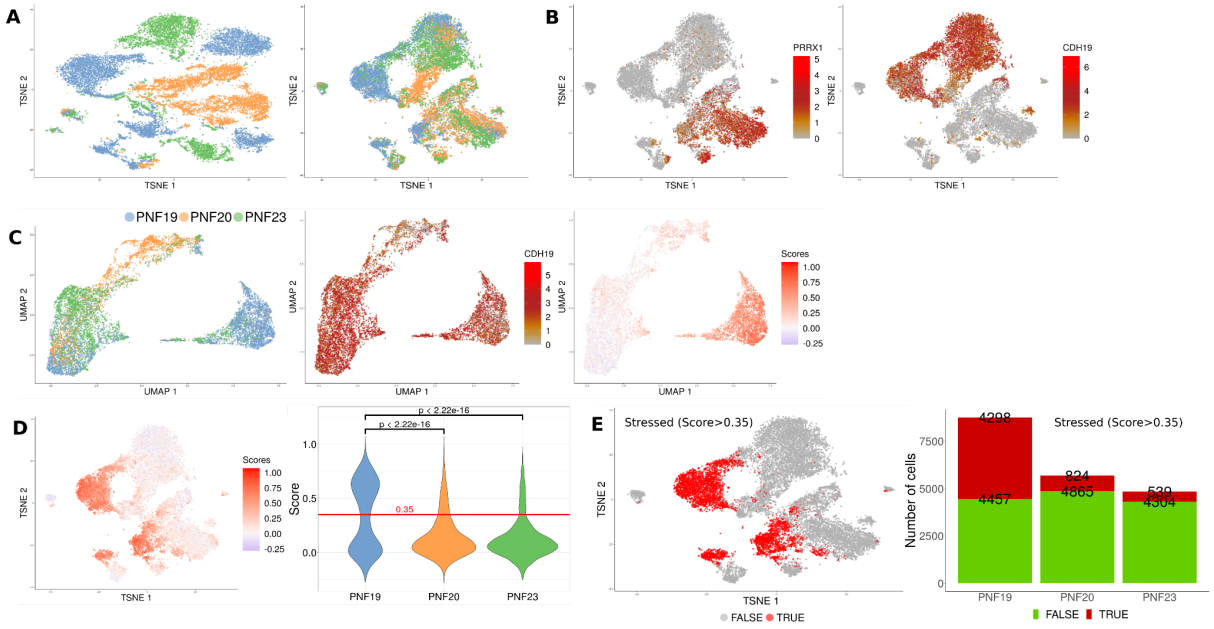

Figure 1. Correction of cellular artifacts among samples is essential for proper downstream analysis

(A) TSNE plots of the whole set of cells, colored by sample of origin, before (left) and after (right) MNN correction.

(B) TSNE plots with cells colored according to the expression of known markers of a mesenchymal component (PRRX1) and the Schwann cell lineage (CDH19).

(C) UMAP representation of the CDH19-expressing component colored by sample of origin (left), CDH19 expression (center), and by the score of the GO:0034976 signature, referring to response to endoplasmic reticulum stress (right).

(D) TSNE representation of the whole set of cells colored by the score of the GO:0034976 signature (left), along with the distribution of the scores across the three samples (right), where we eliminated cells with a score >0.35 from downstream analysis.

(E) Representation of the cells eliminated from downstream analysis (in red), both in the TSNE plot and in a barplot separating per sample.

4.2 Cellular heterogeneity within pNFs

After ensuring that proper quality control and sample cleaning procedures were performed, we moved on to downstream analysis with the now reduced set of cells (Fig. 1E). In Fig. 2A, we can observe the updated TSNE plot after performing MNN correction on the set of cells, where we now see a more homogeneous distribution of the three pNF samples across the space, where despite showing some expected differences between them because of their different biological origins or the stage of tumor development, they all show a very similar pattern (Fig. S3).

Performing clustering on the whole set of cells using a two-step procedure combining k-means and graph-based clustering, we obtained a total of 13 clusters of cells representing different transcriptional profiles (Fig. 2B). Cell type annotation was performed using SingleR and the Human Primary Cell Atlas as a reference, and assigned predicted identities to each of the clusters, which helped in the characterization of the cellular composition of pNFs (Fig. S4). The results showed a quite confident assignment of clusters 1, 3, 6, 7, 9 and 10 to a Schwann cell phenotype, whereas clusters 2, 4, 5 and 11 were assigned to mesenchymal identities. Other less populated clusters were assigned to endothelial cells and various immune cell types.

To further dig into this matter, we assessed the per-cell expression of Schwann cell lineage markers (S100B, CDH19, SOX10), and markers for a mesenchymal phenotype (PRRX1, TWIST1), which went accordingly with the results from the annotations and revealed the presence of two main cellular components expressing markers from one type or the other (Fig. 2C). However, S100B did not show expression in the totality of the clusters assigned to a Schwann cell phenotype, but its expression was rather concentrated in a subset of cells that could therefore represent a more mature SC state. This could be a sign of cellular heterogeneity and suggests for the potential presence of cells at different stages of the NC-SC differentiation axis within pNFs.

Cell type annotations predicted by SingleR were also examined for single cells, where cells were assigned a refined identity label that was then grouped into more general cellular components for visualization purposes. However, the reliability of the annotations using SingleR was a limitation for us, specially due to the lack of a proper transcriptional reference and finer cell type labels specific to the PNS, which made it hard for us to rely solely on these predictions. Also, a considerable proportion of cells in the dataset were labeled by the algorithm as iPSCs, which is obviously a contradiction in the context of primary tumor samples. However, due to the lack of label resolution of the reference used, we considered this label could be identifying cells in a less differentiated state and maintained the original labeling. The grouping of the assigned labels into more general components yielded the identification of 5 different cellular components, consisting of a Schwann cell component, a mesenchymal component, iPS cells, endothelial cells, and immune cells, with the first two being the most abundant.

The distribution of these cellular components projected on the TSNE plot (Fig. 2D) matches with the areas in which our set of selected markers is expressed (Fig. 2C). In contrast with the components of endothelial and immune cells, which do not appear connected in the dimensionally reduced space, the Schwann cell and the mesenchymal components do appear connected on the TSNE plot, a fact that was of interest for us, as it could be an indication of a potential common origin between these two components. A plot of the cell type assignments using more refined labels can also be found in Figure S5.

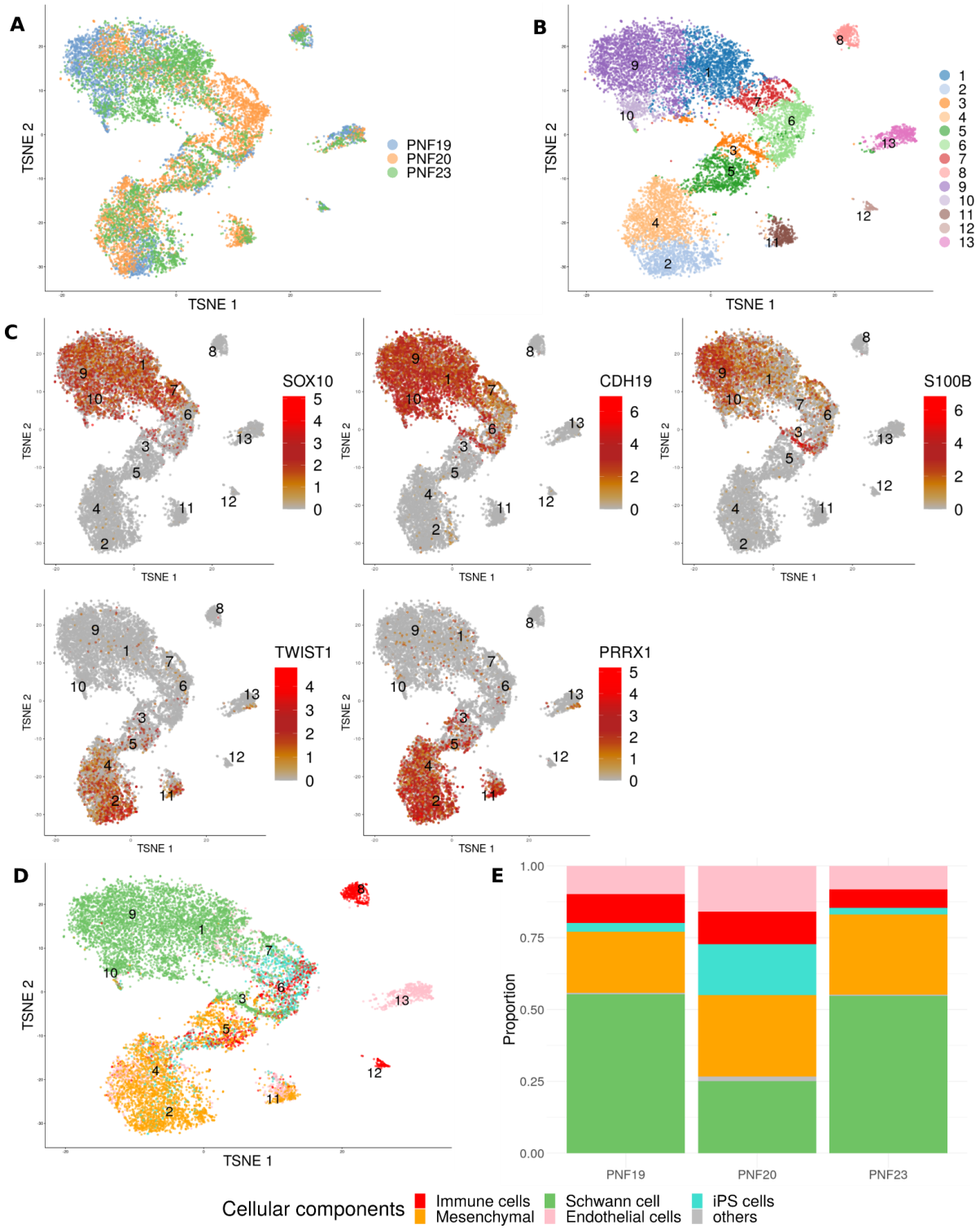

Figure 2. Expression of markers and cell type annotation reveals the main cellular components present in pNFs and their proportions

(A) TSNE plot of the whole set of cells after performing the quality control procedures and MNN correction, colored by sample of origin.

(B) TSNE plot with all cells colored by their assigned cluster, showing 13 clusters of cells, after running k-means + graph-based clustering.

(C) Per-cell expression of Schwann lineage markers (SOX10, CDH19, S100B), and mesenchymal markers (TWIST1, PRRX1) on the TSNE plots, revealing the presence of the two main cellular components present within these tumors.

(D) TSNE plot with cells colored by their assigned cellular identity, after grouping of more refined cellular types into generalized components.

(E) Barplot showing the detected proportions of the main cellular components within each of the three pNF samples.

When looking at the proportions for each of the components (Fig. 2E), we obtain similar results to what we expected according to previous studies on intratumor heterogeneity (Carrió et al., 2018), in which Schwann cells and endoneurial fibroblasts are found to be the most abundant types, respectively. The profiles in cellular composition seem to be consistent across the different samples, except in the case of PNF20, where there seems to be a kind of tradeoff between the proportion of Schwann cells and that of the cells labeled as iPSCs, which could potentially point towards it having a higher proportion of cells with stemness properties, implying that this tumor could be in an active growth phase.

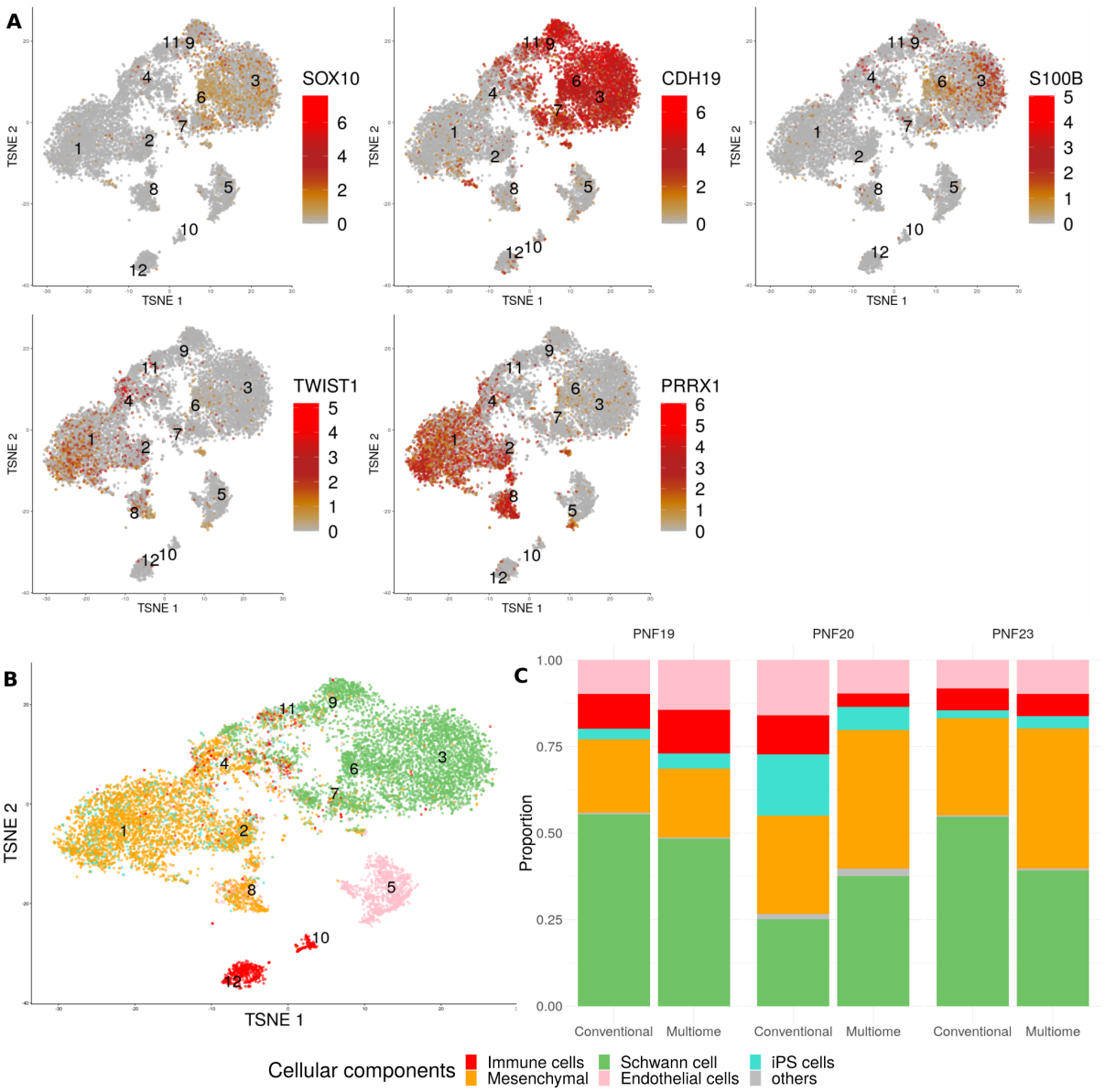

Figure 3. Gene expression analysis with 10X Genomics Multiome yields consistent results when compared to conventional scRNA-seq analysis

(A) Per-cell expression of Schwann lineage markers (S100B, CDH19, SOX10), and mesenchymal markers (PRRX1, TWIST1) on the TSNE plots from the Multiome analysis, consistently revealing the presence of the two main cellular components present within these tumors.

(B) TSNE plot from the Multiome analysis with cells colored by their assigned cellular components, showing a very similar distribution to the one from conventional scRNA-seq analysis.

(C) Barplot showing the detected proportions of the main cellular components within each of the three pNF samples, comparing the results from conventional scRNA-seq analysis and those obtained using Multiome.

When analyzing single-cell gene expression data of a different set of cells from the same pNF samples using the Single Cell Multiome ATAC + Gene Expression technology from 10X Genomics, we had interest in assessing whether we would observe consistent results regarding the heterogeneity of cells composing these tumors with what we had previously seen with conventional scRNA-seq analysis. The data was processed following exactly the same quality control and downstream procedures as explained above. When plotting the per-cell expression of Schwann cell lineage and mesenchymal markers, we again observed the presence of two main components of cells expressing markers from one type or the other, despite showing less intense levels of expression in some cases (Fig. 3A). The results of the cell type annotations using SingleR also led to the identification of the same 5 main cellular components, showing a similar distribution pattern across the dimensionally reduced space (Fig. 3B). In general, the proportions observed for each of the cellular components are consistent with our previous findings (Fig. 3C), and despite showing some differences within each of the samples, the results still match what we expected according to the previous studies mentioned above.

Overall, the results from the single-cell gene expression analysis using the Multiome technology showed consistency with those obtained from conventional scRNA-seq analysis. This validation is of importance for us as it could have practical implications regarding the appropriateness of the approaches used for future research studies. However, the observed variability between both approaches, as well as the lack of intensity in the expression of some genes in the case of the analysis using Multiome are factors to be taken into account.

4.3 Understanding diversity within the Schwann cell component

In Mazuelas et al., 2022, an expression roadmap of NC-SC differentiation was generated in which NC cells were differentiated into SCs and different timepoints were sampled (at 0, 7, 14 and 30 days after the induction of SC differentiation) in order to perform bulk RNA-seq analysis and obtain sets of genes found to be upregulated at the different stages. To study the potential diversity of SCs within pNFs, we made use of these sets of upregulated genes in order to generate signature plots for the different stages on our set of cells in which genes from day 0 were used as a signature for a NC stage, genes from days 7 and 14 were merged to be used as a signature for an Early SC stage, and genes from day 30 were used as a signature for a Mature SC stage. The results of this analysis showed the presence of a clear diversity within the SC component which is due to the presence of cells at different stages of the NC-SC differentiation axis (Figure 4A), as it can be seen how the spatial distribution of the highest scores for the signatures on the TSNE plot moves through the SC component as the stages become more mature. A very similar thing was observed when plotting the per-cell expression of markers for each of the stages (STMN1, EHBP1, and GAS7, respectively), which were selected from the expression roadmap (Figure 4B).

The results from the RNA velocity analysis, which aims to predict the future transcriptional state of single cells, also yielded consistent results with the previous analysis (Figure 4C). It can be observed how there is a very clear and rapid progression of cells within the SC component that seems to have an origin around cluster 6, where then cells progress rapidly and consequently enter in a more steady state around clusters 9 and 10, which matches with the clusters having higher scores for the Mature SC signature. The main strength of this analysis lies on the fact that it works independently to any other information we have previously obtained, as it is solely based on the analysis of the ratio of unspliced to spliced transcripts in order to infer the transcriptional directionality of each cell, which reinforces our previous ideas from a completely different perspective.

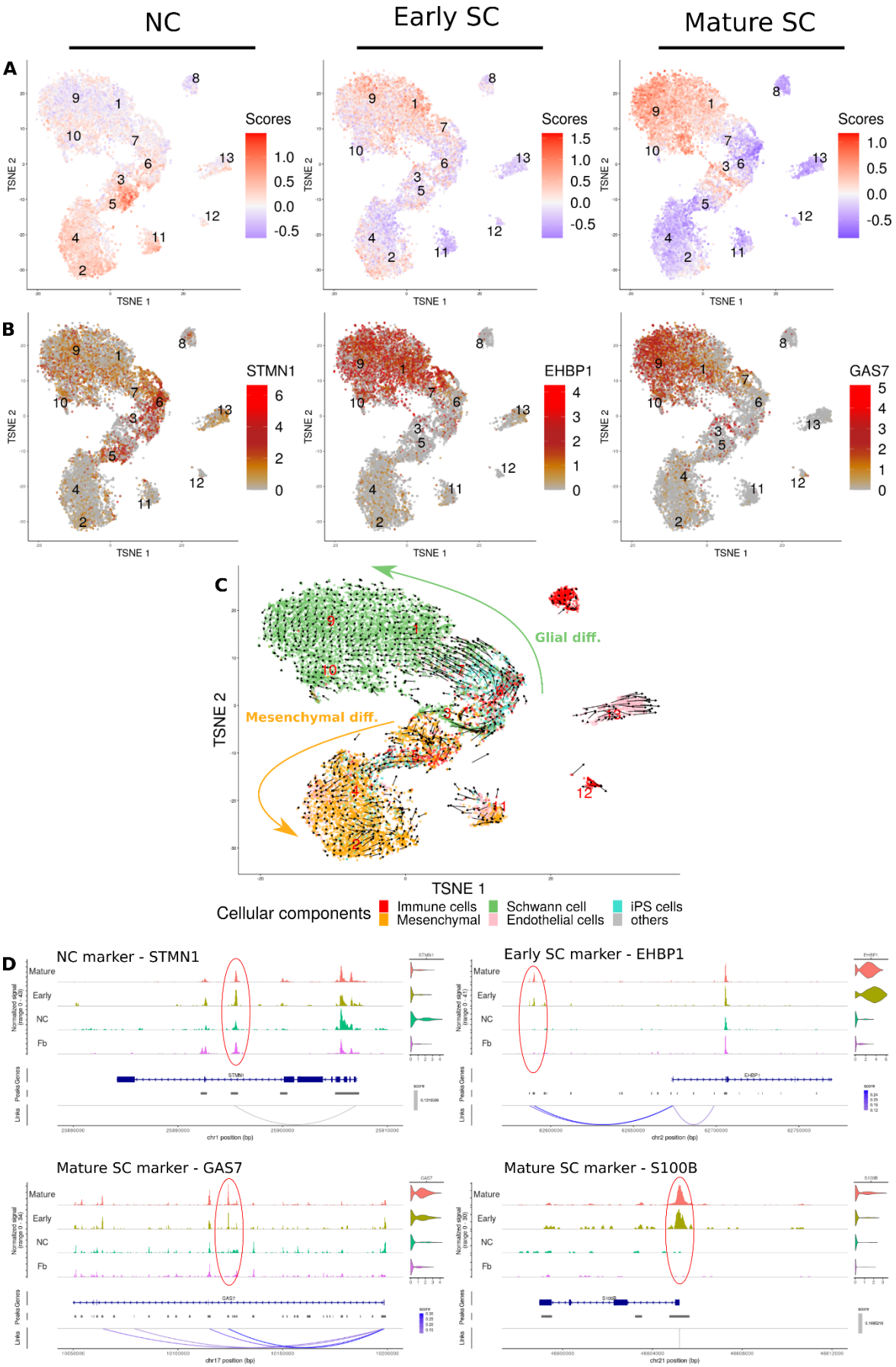

Figure 4. Evaluation of diversity within the SC component reveals the presence of cells at diverse stages of differentiation within the NC-SC axis, which implies transcriptional and epigenetic changes

(legend continued on next page)

Interestingly, we noticed that a similar phenomenon to what we observed within the SC component also happens in the case of the mesenchymal component, where cells seem to progress rapidly across cluster 5 and the amount of change becomes less drastic around clusters 2 and 4, which suggests that a similar progression regarding cells at different stages of differentiation might also be happening within the mesenchymal component. Despite its limitations, this observation, along with the fact that we observe highest scores for a NC signature in what appears to be the origin of this progression in the mesenchymal component (Figure 4A), reinforces the idea given in previous studies that these cells may potentially share a common NC origin with SCs (Joseph et al., 2004).

The scores of the signatures of SC differentiation stages, as well as an extra signature for endoneurial fibroblasts, were used to assign certain cells to a particular state, so that cells that were assigned a high score for the Mature SC signature, for instance, were assigned as Mature SCs, and similarly for the rest of states. With this, we analyzed our single-cell ATAC-seq data from 10X Genomics Multiome in order to compare the chromatin accessibility profiles (represented by peaks) between cells assigned with different cellular states. We generated coverage plots for genomic regions covering the mentioned selected marker genes for the SC differentiation stages to make these comparisons, along with the distribution of their respective expression levels (Figure 4D).

In the case of the NC marker STMN1, the predicted expression-regulating peak is present in all states while the gene is mostly expressed in NC cells. However, in the case of the Early SC marker EHBP1, the peak is only present in the case of Early and Mature SCs, suggesting that there is a change in the chromatin accessibility profile of cells that seems to happen right when cells start their differentiation process from NC towards a mature SC. This chromatin remodeling gives cells within the Schwann cell lineage a defined epigenetic identity. The same thing is observed in the case of Mature SC markers GAS7 and also S100B, where despite being markers that are not yet expressed in the case of Early SCs, the chromatin accessibility profiles of these cells seem to be already prepared to allow cells to express them in the future.This fact reinforces the idea that epigenetic changes are defining the identity of these cells and play an important role in their process of differentiation, but are however not sufficient to infer whether a gene is going to be expressed or not.

4.4 Validation of in vitro 3D neurofibroma models

iPSC-derived 3D neurofibroma models termed neurofibromaspheres have been developed in a recent study in our lab. A more generic analysis of single-cell RNAseq data of 3 of these models was performed in order to assess whether their cellular composition would reproduce that of primary tumors. A combined analysis of both data from primary tumors and 3D models was performed in order to allow us to make comparisons easily, where the data was processed and analyzed following the same procedures explained previously.

When plotting all cells in the TSNE plot, we could observe how cells from the 3D models appeared clearly separated from all cells from primary tumors (Fig. 5A), and how cells from the 3 different 3D models were grouped together despite showing some differences (Fig. S6), just like in the case of the primary tumors. This strong separation could be due to the fact that cells from the models have been cultured *in vitro*, a factor that is known to cause significant differences in the transcriptional profiles of cells compared to primary tumors, according to previous studies (Miller et al. 2009), which

---

(A) TSNE plots with cells colored according to the scores of the signatures of SC differentiation stages: NC (left), Early SC (center), and Mature SC (right).
(B) TSNE plots with the per-cell expression of selected markers for NC (STMN1), Early SC (EHBP1), and Mature SC (GAS7), respectively.
(C) TSNE plot showing the results of the RNA velocity analysis, which infers transcriptional directionality to each cell, with cells colored according to their assigned cellular component.
(D) Coverage plots comparing the chromatin accessibility between different cellular states of key regions with links to markers STMN1, EHBP1, GAS7, and S100B, along with their respective expression levels.

made it really challenging for us to perform further analysis of this data. Despite these difficulties, with the cell type predictions of single cells performed using SingleR (Fig. 5B), we were able to identify the presence of a component of Schwann cells, as well as a component of cells with a mesenchymal phenotype, which are the two components that we expected to find at first glance. We obviously did not identify a component of immune cells or endothelial cells, as these are not included in the generation of neurofibromaspheres. These results were consistent when assessing the expression of markers for the SC lineage and for a mesenchymal phenotype (Fig. 5C), where we were able to identify cells expressing markers from both types, as well as successfully differentiated SCs expressing S100B within the 3D models. Overall, despite the difficulties encountered in terms of proper interpretation of the results of this analysis, we were able to find the expected components of cells within *in vitro* 3D neurofibroma models, as well as observing that they seem to recapitulate the cellular composition found in primary tumors.

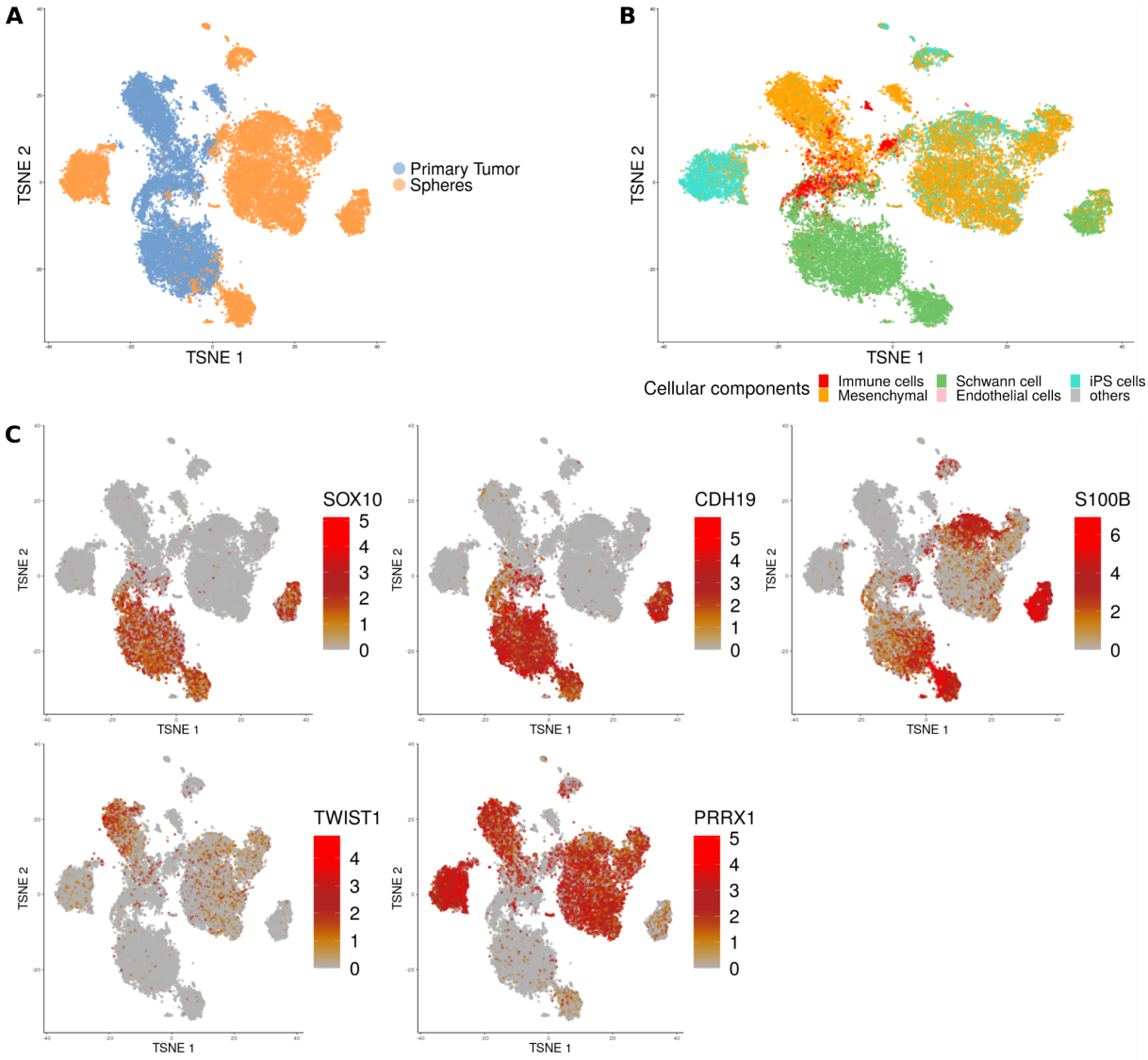

Figure 5. iPSC-based in vitro 3D neurofibroma models seem to recapitulate the cellular composition of primary tumors

(A) TSNE plot with cells from both primary tumors and 3D models (spheres), colored according to their origin.

(B) TSNE plot of the whole set of cells colored by their assigned cellular components, where we are able to identify the main expected components within the 3D neurofibroma models.

(C) Per-cell expression of Schwann lineage markers (SOX10, CDH19, S100B), and mesenchymal markers (TWIST1, PRRX1) on the TSNE plots of the whole set of cells from primary tumors and 3D models.

5.- Conclusions

This study constitutes one of the first in-depth single-cell analysis of pNFs. With it, we have observed the presence of cellular diversity within these tumors, and identified the expected cellular components with their expected proportions, according to previous pathological characterization. Additionally, we found that the heterogeneity that exists within the Schwann cell component is partially due to the presence of cells at different stages of differentiation, which seems to happen in a similar way in the case of the mesenchymal component, reinforcing the idea that these cells may potentially share a common NC origin with SCs. This NC-SC differentiation not only implies transcriptional changes, but also epigenetic changes, which appear to be decoupled from one another.

iPSC-based *in vitro* 3D neurofibroma models generated in the lab also have the expected cellular components and seem to recapitulate the cellular composition found in primary tumors. Also, we concluded that gene expression analysis with 10X Genomics Multiome is comparable with results from conventional scRNA-seq. Finally, we want to emphasize on the importance of performing proper quality control procedures that go beyond the correction of artifacts that might appear during the generation of libraries and sequencing, which is key to ensure the credibility of downstream results.

All in all, tumor analysis at the single cell level can help acquire a better understanding of their underlying biological structure and shed some light on which are the mechanisms by which these tumors arise and develop.

Acknowledgements

I would like to thank my supervisors Bernat Gel and Eduard Serra for their constant guidance throughout these past months, and also every member of the Hereditary Cancer Group at IGTP. Thank you. For the opportunity, for your unconditional help, for providing me with an amazing work environment which has made me feel so comfortable, for helping me grow along with your knowledge, not only academically but most importantly as a person. Thank you, for making this possible. I wish you all the best for the future.

To my parents, friends, and to you, for hanging in there.

Funding

This work has been supported by the Instituto de Salud Carlos III National Health Institute funded by FEDER funds—a way to build Europe—[PI14/00577, PI17/00524, PI19/00553, PI20/00228]; Department of Defense office of the Congressionally Directed Medical Research Programs (CDMRP) NFRP FY20 (NF200051); Fundación PROYECTO NEUROFIBROMATOSIS; the Government of Catalonia [2017-SGR-496], CERCA Program; Fundació La Marató de TV3 (51/C/2019).

Bibliography

Aran, D., Looney, A. P., Liu, L., Wu, E., Fong, V., Hsu, A., Chak, S., Naikawadi, R. P., Wolters, P. J., Abate, A. R., Butte, A. J., & Bhattacharya, M. (2019). Reference-based analysis of lung single-cell sequencing reveals a transitional profibrotic macrophage. *Nature Immunology*, *20*(2), 163–172. https://doi.org/10.1038/s41590-018-0276-y

Beert, E., Brems, H., Daniëls, B., De Wever, I., Van Calenbergh, F., Schoenaers, J., Debiec-Rychter, M., Gevaert, O., De Raedt, T., Van Den Bruel, A., de Ravel, T., Cichowski, K., Kluwe, L., Mautner, V., Sciot, R., & Legius, E. (2011). Atypical neurofibromas in neurofibromatosis type 1 are premalignant tumors. *Genes, Chromosomes and Cancer*, *50*(12), 1021–1032. https://doi.org/10.1002/gcc.20921

Bergen, V., Lange, M., Peidli, S., Wolf, F. A., & Theis, F. J. (2019). *Generalizing RNA velocity to transient cell states through dynamical modeling* [Preprint]. Bioinformatics. https://doi.org/10.1101/820936

Bray, N. L., Pimentel, H., Melsted, P., & Pachter, L. (2016). Near-optimal probabilistic RNA-seq quantification. *Nature Biotechnology*, *34*(5), 525–527. https://doi.org/10.1038/nbt.3519

Brems, H., Park, C., Maertens, O., Pemov, A., Messiaen, L., Upadhyaya, M., Claes, K., Beert, E., Peeters, K., Mautner, V., Sloan, J. L., Yao, L., Lee, C.-C. R., Sciot, R., De Smet, L., Legius, E., & Stewart, D. R. (2009). Glomus Tumors in Neurofibromatosis Type 1: Genetic, Functional, and Clinical Evidence of a Novel Association. *Cancer Research*, *69*(18), 7393–7401. https://doi.org/10.1158/0008-5472.CAN-09-1752

Buchstaller, J., Clapp, D. W., Parada, L. F., & Zhu, Y. (2012). Cell of Origin and the Contribution of Microenvironment in NF1 Tumorigenesis and Therapeutic Implications. In M. Upadhyaya & D. N. Cooper (Eds.), *Neurofibromatosis Type 1* (pp. 549–568). Springer Berlin Heidelberg.

https://doi.org/10.1007/978-3-642-32864-0_36

Carli, M., Ferrari, A., Mattke, A., Zanetti, I., Casanova, M., Bisogno, G., Cecchetto, G., Alaggio, R., De Sio, L., Koscielniak, E., Sotti, G., & Treuner, J. (2005). Pediatric Malignant Peripheral Nerve Sheath Tumor: The Italian and German Soft Tissue Sarcoma Cooperative Group. *Journal of Clinical Oncology*, *23*(33), 8422–8430. https://doi.org/10.1200/JCO.2005.01.4886

Carrió, M., Gel, B., Terribas, E., Zucchiatti, A. C., Moliné, T., Rosas, I., Teulé, Á., Ramón y Cajal, S., López-Gutiérrez, J. C., Blanco, I., Castellanos, E., Lázaro, C., Stemmer-Rachamimov, A., Romagosa, C., & Serra, E. (2018). Analysis of intratumor heterogeneity in Neurofibromatosis type 1 plexiform neurofibromas and neurofibromas with atypical features: Correlating histological and genomic findings. *Human Mutation*, *39*(8), 1112–1125. https://doi.org/10.1002/humu.23552

Chen, Z., Liu, C., Patel, A. J., Liao, C.-P., Wang, Y., & Le, L. Q. (2014). Cells of Origin in the Embryonic Nerve Roots for NF1-Associated Plexiform Neurofibroma. *Cancer Cell*, *26*(5), 695–706. https://doi.org/10.1016/j.ccell.2014.09.009

Dombi, E., Baldwin, A., Marcus, L. J., Fisher, M. J., Weiss, B., Kim, A., Whitcomb, P., Martin, S., Aschbacher-Smith, L. E., Rizvi, T. A., Wu, J., Ershler, R., Wolters, P., Therrien, J., Glod, J., Belasco, J. B., Schorry, E., Brofferio, A., Starosta, A. J., … Widemann, B. C. (2016). Activity of Selumetinib in Neurofibromatosis Type 1–Related Plexiform Neurofibromas. *New England Journal of Medicine*, *375*(26), 2550–2560. https://doi.org/10.1056/NEJMoa1605943

Dombi, E., Solomon, J., Gillespie, A. J., Fox, E., Balis, F. M., Patronas, N., Korf, B. R., Babovic-Vuksanovic, D., Packer, R. J., Belasco, J., Goldman, S., Jakacki, R., Kieran, M., Steinberg, S. M., & Widemann, B. C. (2007). NF1 plexiform neurofibroma growth rate by volumetric MRI: Relationship to age and body weight. *Neurology*, *68*(9), 643–647. https://doi.org/10.1212/01.wnl.0000250332.89420.e6

Ducatman, B. S., Scheithauer, B. W., Piepgras, D. G., Reiman, H. M., & Ilstrup, D. M. (1986). Malignant peripheral nerve sheath tumors. A clinicopathologic study of 120 cases. *Cancer*, *57*(10), 2006–2021. https://doi.org/10.1002/1097-0142(19860515)57:10<2006::AID-CNCR2820571022>3.0.CO;2-6

Evans, D. G. R., O'Hara, C., Wilding, A., Ingham, S. L., Howard, E., Dawson, J., Moran, A., Scott-Kitching, V., Holt, F., & Huson, S. M. (2011). Mortality in neurofibromatosis 1: In North West England: an assessment of actuarial survival in a region of the UK since 1989. *European Journal of Human Genetics*, *19*(11), 1187–1191. https://doi.org/10.1038/ejhg.2011.113

Ferner, R. E. (2007). Neurofibromatosis 1 and neurofibromatosis 2: A twenty first century perspective. *The Lancet Neurology*, *6*(4), 340–351. https://doi.org/10.1016/S1474-4422(07)70075-3

Ge, S. X., Jung, D., & Yao, R. (2020). ShinyGO: A graphical gene-set enrichment tool for animals and plants. *Bioinformatics*, *36*(8), 2628–2629. https://doi.org/10.1093/bioinformatics/btz931

Germain, P.-L., Lun, A., Macnair, W., & Robinson, M. D. (2021). Doublet identification in single-cell sequencing data using scDblFinder. *F1000Research*, *10*, 979. https://doi.org/10.12688/f1000research.73600.1

Griffiths, J. A., Richard, A. C., Bach, K., Lun, A. T. L., & Marioni, J. C. (2018). Detection and removal of barcode swapping in single-cell RNA-seq data. *Nature Communications*, *9*(1), 2667. https://doi.org/10.1038/s41467-018-05083-x

Haghverdi, L., Lun, A. T. L., Morgan, M. D., & Marioni, J. C. (2018). Batch effects in single-cell RNA-sequencing data are corrected by matching mutual nearest neighbors. *Nature Biotechnology*, *36*(5), 421–427. https://doi.org/10.1038/nbt.4091

Hao, Y., Hao, S., Andersen-Nissen, E., Mauck, W. M., Zheng, S., Butler, A., Lee, M. J., Wilk, A. J., Darby, C., Zager, M., Hoffman, P., Stoeckius, M., Papalexi, E., Mimitou, E. P., Jain, J., Srivastava, A., Stuart, T., Fleming, L. M., Yeung, B., … Satija, R. (2021). Integrated analysis of multimodal single-cell data. *Cell*, *184*(13), 3573-3587.e29. https://doi.org/10.1016/j.cell.2021.04.048

Hirbe, A. C., Dahiya, S., Miller, C. A., Li, T., Fulton, R. S., Zhang, X., McDonald, S., DeSchryver, K., Duncavage, E. J., Walrath, J., Reilly, K. M., Abel, H. J., Pekmezci, M., Perry, A., Ley, T. J., & Gutmann, D. H. (2015). Whole Exome Sequencing Reveals the Order of Genetic Changes during Malignant Transformation and Metastasis in a Single Patient with NF1-plexiform Neurofibroma. *Clinical Cancer Research*, *21*(18), 4201–4211. https://doi.org/10.1158/1078-0432.CCR-14-3049

Huber, W., Carey, V. J., Gentleman, R., Anders, S., Carlson, M., Carvalho, B. S., Bravo, H. C., Davis, S., Gatto, L., Girke, T., Gottardo, R., Hahne, F., Hansen, K. D., Irizarry, R. A., Lawrence, M., Love, M. I., MacDonald, J., Obenchain, V., Oleś, A. K., … Morgan, M. (2015). Orchestrating high-throughput genomic analysis with Bioconductor. *Nature Methods*, *12*(2), 115–121. https://doi.org/10.1038/nmeth.3252

Joseph, N. M., Mukouyama, Y., Mosher, J. T., Jaegle, M., Crone, S. A., Dormand, E.-L., Lee, K.-F., Meijer, D., Anderson, D. J., & Morrison, S. J. (2004). Neural crest stem cells undergo multilineage differentiation in developing peripheral nerves to generate endoneurial fibroblasts in addition to Schwann cells. *Development*, *131*(22), 5599–5612. https://doi.org/10.1242/dev.01429

Krone, W., Jirikowski, G., M&#xFFFD;hleck, O., Kling, H., & Gall, H. (1983). Cell culture studies on neurofibromatosis (von Recklinghausen). II. Occurrence of glial cells in primary cultures of peripheral neurofibromas. *Human Genetics*, *63*(3). https://doi.org/10.1007/BF00284658

Lun, A. T. L., McCarthy, D. J., & Marioni, J. C. (2016). A step-by-step workflow for low-level analysis of single-cell RNA-seq data with Bioconductor. *F1000Research*, *5*, 2122. https://doi.org/10.12688/f1000research.9501.2

Mabbott, N. A., Baillie, J., Brown, H., Freeman, T. C., & Hume, D. A. (2013). An expression atlas of human primary cells: Inference of gene function from coexpression networks. *BMC Genomics*, *14*(1), 632. https://doi.org/10.1186/1471-2164-14-632

Mautner, V.-F., Asuagbor, F. A., Dombi, E., Fünsterer, C., Kluwe, L., Wenzel, R., Widemann, B. C., & Friedman, J. M. (2008). Assessment of benign tumor burden by whole-body MRI in patients with neurofibromatosis 1. *Neuro-Oncology*, *10*(4), 593–598. https://doi.org/10.1215/15228517-2008-011

Mazuelas, H., Carrió, M., & Serra, E. (2020). Modeling tumors of the peripheral nervous system associated with Neurofibromatosis type 1: Reprogramming plexiform neurofibroma cells. *Stem Cell Research*, *49*, 102068. https://doi.org/10.1016/j.scr.2020.102068

Mazuelas, H., Magallón-Lorenz, M., Fernández-Rodríguez, J., Uriarte-Arrazola, I., Richaud-Patin, Y., Terribas, E., Villanueva, A., Castellanos, E., Blanco, I., Raya, Á., Chojnacki, J., Heyn, H., Romagosa, C., Lázaro, C., Gel, B., Carrió, M., & Serra, E. (2022). Modeling iPSC-derived human neurofibroma-like tumors in mice uncovers the heterogeneity of Schwann cells within plexiform neurofibromas. *Cell Reports*, *38*(7), 110385.

https://doi.org/10.1016/j.celrep.2022.110385

McCarthy, D. J., Campbell, K. R., Lun, A. T. L., & Wills, Q. F. (2017). Scater: Pre-processing, quality control, normalization and visualization of single-cell RNA-seq data in R. *Bioinformatics*, btw777. https://doi.org/10.1093/bioinformatics/btw777

Melsted, P., Booeshaghi, A. S., Liu, L., Gao, F., Lu, L., Min, K. H., da Veiga Beltrame, E., Hjörleifsson, K. E., Gehring, J., & Pachter, L. (2021). Modular, efficient and constant-memory single-cell RNA-seq preprocessing. *Nature Biotechnology*, *39*(7), 813–818. https://doi.org/10.1038/s41587-021-00870-2

Miller, S. J., Jessen, W. J., Mehta, T., Hardiman, A., Sites, E., Kaiser, S., Jegga, A. G., Li, H., Upadhyaya, M., Giovannini, M., Muir, D., Wallace, M. R., Lopez, E., Serra, E., Nielsen, G. P., Lazaro, C., Stemmer‐Rachamimov, A., Page, G., Aronow, B. J., & Ratner, N. (2009). Integrative genomic analyses of neurofibromatosis tumours identify SOX9 as a biomarker and survival gene. *EMBO Molecular Medicine*, *1*(4), 236–248. https://doi.org/10.1002/emmm.200900027

Miller, S. J., Rangwala, F., Williams, J., Ackerman, P., Kong, S., Jegga, A. G., Kaiser, S., Aronow, B. J., Frahm, S., Kluwe, L., Mautner, V., Upadhyaya, M., Muir, D., Wallace, M., Hagen, J., Quelle, D. E., Watson, M. A., Perry, A., Gutmann, D. H., & Ratner, N. (2006). Large-Scale Molecular Comparison of Human Schwann Cells to Malignant Peripheral Nerve Sheath Tumor Cell Lines and Tissues. *Cancer Research*, *66*(5), 2584–2591. https://doi.org/10.1158/0008-5472.CAN-05-3330

Ortonne, N., Wolkenstein, P., Blakeley, J. O., Korf, B., Plotkin, S. R., Riccardi, V. M., Miller, D. C., Huson, S., Peltonen, J., Rosenberg, A., Carroll, S. L., Verma, S. K., Mautner, V., Upadhyaya, M., & Stemmer-Rachamimov, A. (2018). Cutaneous neurofibromas: Current clinical and pathologic issues. *Neurology*, *91*(2 Supplement 1), S5–S13. https://doi.org/10.1212/WNL.0000000000005792

Pemov, A., Li, H., Patidar, R., Hansen, N. F., Sindiri, S., Hartley, S. W., Wei, J. S., Elkahloun, A., Chandrasekharappa, S. C., NISC Comparative Sequencing Program, Boland, J. F., Bass, S., NCI DCEG Cancer Genomics Research Laboratory, Mullikin, J. C., Khan, J., Widemann, B. C., Wallace, M. R., & Stewart, D. R. (2017). The primacy of NF1 loss as the driver of tumorigenesis in neurofibromatosis type 1-associated plexiform neurofibromas. *Oncogene*, *36*(22), 3168–3177. https://doi.org/10.1038/onc.2016.464

Prada, C. E., Rangwala, F. A., Martin, L. J., Lovell, A. M., Saal, H. M., Schorry, E. K., & Hopkin, R. J. (2012). Pediatric Plexiform Neurofibromas: Impact on Morbidity and Mortality in Neurofibromatosis Type 1. *The Journal of Pediatrics*, *160*(3), 461–467. https://doi.org/10.1016/j.jpeds.2011.08.051

Ratner, N., & Miller, S. J. (2015). A RASopathy gene commonly mutated in cancer: The neurofibromatosis type 1 tumour suppressor. *Nature Reviews Cancer*, *15*(5), 290–301. https://doi.org/10.1038/nrc3911

Riccardi, V. M. (1992). Type 1 neurofibromatosis and the pediatric patient. *Current Problems in Pediatrics*, *22*(2), 66–106. https://doi.org/10.1016/0045-9380(92)90053-2

Ritchie, M. E., Phipson, B., Wu, D., Hu, Y., Law, C. W., Shi, W., & Smyth, G. K. (2015). Limma powers differential expression analyses for RNA-sequencing and microarray studies. *Nucleic Acids Research*, *43*(7), e47–e47. https://doi.org/10.1093/nar/gkv007

Serra, E. (2000). Schwann cells harbor the somatic NF1 mutation in neurofibromas: Evidence of two different Schwann cell subpopulations. *Human Molecular Genetics*, *9*(20), 3055–3064. https://doi.org/10.1093/hmg/9.20.3055

Serra, E., Gel, B., Fernández-Rodríguez, J., & Lázaro, C. (2020). Genomics of Peripheral Nerve Sheath Tumors Associated with Neurofibromatosis Type 1. In G. Tadini, E. Legius, & H. Brems (Eds.), *Multidisciplinary Approach to Neurofibromatosis Type 1* (pp. 117–147). Springer International Publishing. https://doi.org/10.1007/978-3-319-92450-2_9

Soldatov, R., Kaucka, M., Kastriti, M. E., Petersen, J., Chontorotzea, T., Englmaier, L., Akkuratova, N., Yang, Y., Häring, M., Dyachuk, V., Bock, C., Farlik, M., Piacentino, M. L., Boismoreau, F., Hilscher, M. M., Yokota, C., Qian, X., Nilsson, M., Bronner, M. E., … Adameyko, I. (2019). Spatiotemporal structure of cell fate decisions in murine neural crest. *Science*, *364*(6444), eaas9536. https://doi.org/10.1126/science.aas9536

Stuart, T., Srivastava, A., Madad, S., Lareau, C. A., & Satija, R. (2021). Single-cell chromatin state analysis with Signac. *Nature Methods*, *18*(11), 1333–1341. https://doi.org/10.1038/s41592-021-01282-5

Uusitalo, E., Rantanen, M., Kallionpää, R. A., Pöyhönen, M., Leppävirta, J., Ylä-Outinen, H., Riccardi, V. M., Pukkala, E., Pitkäniemi, J., Peltonen, S., & Peltonen, J. (2016). Distinctive Cancer Associations in Patients With Neurofibromatosis Type 1. *Journal of Clinical Oncology*, *34*(17), 1978–1986. https://doi.org/10.1200/JCO.2015.65.3576

Wickham, H. (2016). *ggplot2: Elegant Graphics for Data Analysis* (2nd ed. 2016). Springer International Publishing : Imprint: Springer. https://doi.org/10.1007/978-3-319-24277-4

Woodhoo, A., & Sommer, L. (2008). Development of the Schwann cell lineage: From the neural crest to the myelinated nerve. *Glia*, *56*(14), 1481–1490. https://doi.org/10.1002/glia.20723

Wu, J., Williams, J. P., Rizvi, T. A., Kordich, J. J., Witte, D., Meijer, D., Stemmer-Rachamimov, A. O., Cancelas, J. A., & Ratner, N. (2008). Plexiform and Dermal Neurofibromas and Pigmentation Are Caused by Nf1 Loss in Desert Hedgehog-Expressing Cells. *Cancer Cell*, *13*(2), 105–116. https://doi.org/10.1016/j.ccr.2007.12.027

Zhang, Y., Liu, T., Meyer, C. A., Eeckhoute, J., Johnson, D. S., Bernstein, B. E., Nusbaum, C., Myers, R. M., Brown, M., Li, W., & Liu, X. S. (2008). Model-based Analysis of ChIP-Seq (MACS). *Genome Biology*, *9*(9), R137. https://doi.org/10.1186/gb-2008-9-9-r137

Zheng, H., Chang, L., Patel, N., Yang, J., Lowe, L., Burns, D. K., & Zhu, Y. (2008). Induction of Abnormal Proliferation by Nonmyelinating Schwann Cells Triggers Neurofibroma Formation. *Cancer Cell*, *13*(2), 117–128. https://doi.org/10.1016/j.ccr.2008.01.002

Zhu, Y., Ghosh, P., Charnay, P., Burns, D. K., & Parada, L. F. (2002). Neurofibromas in NF1: Schwann Cell Origin and Role of Tumor Environment. *Science*, *296*(5569), 920–922. https://doi.org/10.1126/science.1068452